Mukhanova, Ekaterina; Zeng, Weijun; Heredia, Elica Anne; Wu, Chun Wei; Lilja, Ilari; Lin, Juhn Jong; Yeh, Sheng Shiuan; Hakonen, Pertti

Kinetic inductance in superconducting $CoSi_2$ coplanar microwave transmission lines

Published in:
APL Materials

DOI:
10.1063/5.0195106

Published: 01/04/2024

Document Version
Publisher's PDF, also known as Version of record

Please cite the original version:
Mukhanova, E., Zeng, W., Heredia, E. A., Wu, C. W., Lilja, I., Lin, J. J., Yeh, S. S., & Hakonen, P. (2024). Kinetic inductance in superconducting $CoSi_2$ coplanar microwave transmission lines. *APL Materials*, *12*(4), 1-7. Article 041115. https://doi.org/10.1063/5.0195106

RESEARCH ARTICLE | APRIL 15 2024

Kinetic inductance in superconducting $CoSi_2$ coplanar microwave transmission lines

Ekaterina Mukhanova ; Weijun Zeng ; Elica Anne Heredia; Chun-Wei Wu; Ilari Lilja; Juhn-Jong Lin ; Sheng-Shiuan Yeh ; Pertti Hakonen

APL Mater. 12, 041115 (2024)
https://doi.org/10.1063/5.0195106

APL Materials | ARTICLE | pubs.aip.org/aip/apm

Kinetic inductance in superconducting $CoSi_2$ coplanar microwave transmission lines

Cite as: APL Mater. 12, 041115 (2024); doi: 10.1063/5.0195106
Submitted: 30 December 2023 • Accepted: 26 March 2024 •
Published Online: 15 April 2024

Ekaterina Mukhanova,[1,2] Weijun Zeng,[1,2] Elica Anne Heredia,[3] Chun-Wei Wu,[4] Ilari Lilja,[1,2] Juhn-Jong Lin,[4] Sheng-Shiuan Yeh,[3,5,a)] and Pertti Hakonen[1,2,a)]

AFFILIATIONS

[1] Low Temperature Laboratory, Department of Applied Physics, Aalto University, P.O. Box 15100, FI-00076 Espoo, Finland
[2] QTF Centre of Excellence, Department of Applied Physics, Aalto University, P.O. Box 15100, FI-00076 Aalto, Finland
[3] International College of Semiconductor Technology, National Yang Ming Chiao Tung University, Hsinchu 30010, Taiwan
[4] Department of Electrophysics, National Yang Ming Chiao Tung University, Hsinchu 30010, Taiwan
[5] Center for Emergent Functional Matter Science, National Yang Ming Chiao Tung University, Hsinchu 30010, Taiwan

[a)] **Authors to whom correspondence should be addressed:** ssyeh@nycu.edu.tw and pertti.hakonen@aalto.fi

ABSTRACT

We have looked into cobalt disilicide ($CoSi_2$) as a potential building block for superconducting quantum circuits. In order to achieve this, we annealed a thin layer of Co to create microwave cavities with thickness of d = 10–105 nm from $CoSi_2$ embedded in the silicon substrate. The cavity properties were measured as a function of temperature and power. In the films measuring 10 and 25 nm, we find a significant kinetic inductance L_K with a non-BCS power-law variation $\delta L_K \propto T^{4.3\pm0.2}$ at low temperatures. The quality factor of the studied microwave resonances varied from 3×10^3 (d = 10 nm) to ~5×10^4 (d = 105 nm) and increased as $d(A - \log d)$ with thickness, with two-level systems having very little effect. The power dependence of kinetic inductance was analyzed in terms of heat flow due to electron–phonon coupling, which was found to be stronger than estimated for heat relaxation by regular quasiparticles.

I. INTRODUCTION

Microwave cavities are essential building blocks for quantum circuits and circuit quantum electrodynamics.[1] Their low-frequency noise properties[2] and dissipation at GHz frequencies[3] will influence, for example, qubit decoherence, which, in turn, causes errors in qubit gates and degrades the single-shot readout efficiency. In addition to the high quality of the fabrication material,[4] the material's compatibility for circuit fabrication is an essential asset for its utilization in very-large-scale integration technology for superconducting circuits.[5]

In this work, we investigate the potential of cobalt disilicide ($CoSi_2$) as a high-quality material for quantum circuits. The cobalt silicide technology has been used for mass production of complementary metal–oxide–semiconductor (CMOS) ultra-large-scale integration (ULSI) in several technology generations from 180 to 65 nm.[6] Silicides, for example, vanadium silicide,[7] are known to be promising materials for silicon-based superconducting field effect transistors, provided that the problem of Schottky barriers is overcome.[8] A cobalt disilicide conductor is a low-temperature superconductor that can be obtained straightforwardly by annealing a stripe of cobalt laid on top of the silicon substrate. The induced chemical reaction is self-limiting, and it results in a high-quality, nearly epitaxial $CoSi_2$ film with excellent lattice match to silicon. Owing to the excellent lattice match, the amount of disorder is small at the $CoSi_2$/Si interface, which promises low $1/f$ noise in this material.[9]

Thin $CoSi_2$ films possess a substantial kinetic inductance. This inductance is related to the normal state resistance R_n, which is known to display low-frequency resistance fluctuations $(\delta R_n)^2 \propto R_n^2$ with a $1/f$ power spectrum.[2] The $1/f$ resistance noise of 105-nm-thick $CoSi_2$ films has been investigated in Ref. 9, and the noise was found to be quite small. One of the questions that we address is whether large kinetic inductance can be achieved in $CoSi_2$ without enhanced dissipation at microwave frequencies, typically caused by the presence of two-level tunneling states (TLS).[3,10] A high-quality

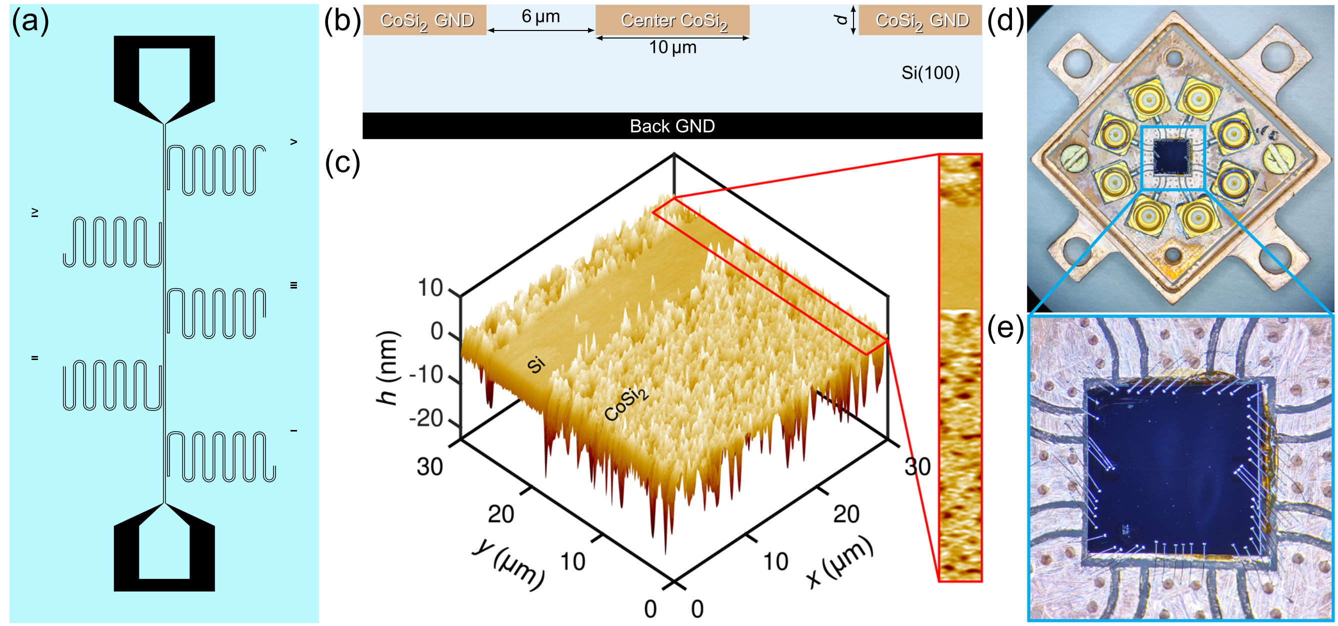

FIG. 1. (a) Notch-type resonator layout with five cavities of slightly different lengths. (b) The cross-sectional view illustrates the ensuing sample structure. (c) AFM image of the surface structure of our 25 nm thick cavity: Si and $CoSi_2$ are marked in the image, (d) and (e) show one cavity sample wire-bonded in the sample box.

superconductor with large kinetic inductance would facilitate, for example, wide-band traveling wave parametric amplifiers.[11,12]

The kinetic inductance for a superconducting wire with the length $L_{\rm line}$ is given near zero temperature by[13]

$$L_{\rm K} = \frac{2}{3\sqrt{3}} \frac{L_{\rm line}}{\xi} \frac{\hbar}{2eI_{\rm c}} = \frac{\hbar R_{\rm n}}{\pi \Delta}. \tag{1}$$

In the latter form, Δ denotes the superconducting gap and $R_{\rm n}$ denotes the total normal-state resistance of the sample. We have employed the fact that according to the Ambegaokar–Baratoff type of relation, the product $R_{\rm n}(\xi)I_{\rm c} = \frac{\pi}{3\sqrt{3}}\Delta/e$ (Ref. 14), where $R_{\rm n}(\xi)$ denotes the resistance of a film section of coherence length ξ; for $CoSi_2$, the superconducting coherence length at zero temperature is $\xi(0) = 90$ nm.[15] Consequently, the kinetic inductance in thin $CoSi_2$ films is enhanced both by increased film resistance and the reduced transition temperature. At finite temperatures, there is a correction $\propto \tanh{(\Delta/k_{\rm B}T)}^{-1}$ (Refs. 16 and 17), which is insignificant in our analysis and has been omitted.

II. SAMPLE FABRICATION AND CHARACTERISTICS

Our samples use a regular notch-type design with five cavities in parallel, as shown in Fig. 1(a). A cobalt film was deposited via thermal evaporation onto a surface area of an undoped Si(100) substrate defined by photolithography. Before the deposition, the native SiO_2 on the substrate surface was removed by soaking it in an aqueous hydrogen fluoride (HF) solution (volume ratio 1.5%) for 3 min. The timing of HF treatment relative to the subsequent evacuation in the thermal evaporator was controlled within 10 min to minimize the regrowth of native SiO_2. It was found the residual photoresist on the substrate surface could significantly hamper the quality (resistivity) of the grown $CoSi_2$ films, and therefore, we applied O_2 plasma treatment after the development to remove the photoresist residuals. These processes lead to good reproducibility of our devices. The deposited Co film was annealed in a vacuum with a pressure of $\sim 1 \times 10^{-6}$ Torr for silicidation. During the thermal annealing process, Co atoms act as predominant moving species, diffusing downward and reacting with Si atoms to form the epitaxial $CoSi_2$ film.[9,18] The silicide thickness ratio for $CoSi_2$/Co is ≈ 3.5 (see Table 8.2 in Ref. 19), i.e., for a Co film with thickness $t_{\rm Co}$, after silicidation, the thickness of $CoSi_2$ is $\approx 3.5 t_{\rm Co}$. A cross-sectional view of our device structure is schematically shown in Fig. 1(b). The transmission electron microscopy (TEM) images in our previous work reveal the epitaxial nature at the $CoSi_2$/Si interface.[9]

In this work, we deposited Co films with thicknesses of 3, 7, 17, and 30 nm, and the expected thicknesses for $CoSi_2$ films are ≈ 10, ≈ 25, ≈ 60, and ≈ 105 nm, respectively. The annealing conditions for 3, 7, 17, and 30 nm thick Co films are 550 °C (30 min) followed by 600 °C (30 min), 600 °C (30 min) followed by 700 °C (30 min), 600 °C (1 h) followed by 700 °C (1 h), and 700 °C (1 h) followed by 800 °C (1 h), respectively. Figure 1(c) shows an AFM image of the surface roughness in our 25 nm thick samples. The measured root mean square (rms) roughness of the $CoSi_2$ surface (excluding the edges with extra spikes) amounts to 1.56, 1.73, 1.51, and 1.78 nm for the samples with the thickness of 10, 25, 60, and 105 nm, respectively. The superconducting temperatures $T_{\rm c}$ were determined by measuring the temperature dependence of resistance at low T using a ^{3}He cryostat. $T_{\rm c}$ is 1.37, 1.31, 1.45, and 1.35 K for the $CoSi_2$ films with thicknesses of $d = 10$, 25, 60, and 105 nm, respectively. The normal-state sheet resistances $R_{\rm s}$ at 1.5 K are 7.1, 2.4, 0.7, and 0.24 Ω, respectively. These values are consistent with those in our previous work,[20] confirming the good reproducibility of our devices. Table I

TABLE I. $CoSi_2$ fabrication parameters and basic characteristics.

t_{CoSi_2}/nm	t_{Co}/nm	T_{anneal}/°C	t_{anneal}/min	T_c/K	R_s/Ω
≈10	3	550 and 600	30 and 30	1.37	7.1
≈25	7	600 and 700	30 and 30	1.31	2.4
≈60	17	600 and 700	60 and 60	1.45	0.7
≈105	30	700 and 800	60 and 60	1.35	0.24

presents the fabrication parameters and basic characteristics of our samples.

Nominally, the cavities have a characteristic impedance of 50 Ω, but this is only valid when the kinetic inductance can be neglected in the design ($d \gtrsim 100$ nm). We chose a width of 10 μm for the center conductor on a high-purity silicon substrate, for which a 6 μm gap between the center conductor and the ground plane corresponds to a 50 Ω transmission line. Afterward, using the measured kinetic inductance, we may state the actual estimates for characteristic impedance as 88, 65, 55, and 50 Ω for 10, 25, 60, and 105 nm thicknesses, respectively. We note that the ground plane conductor is made of the same material, which means that the ground plane does contain significant kinetic inductance for our 10 and 25 nm resonators, but this was neglected in our analysis.

III. EXPERIMENTAL METHODS

Our samples were bonded to sample boxes using a 25 μm Al wire with three wires connecting both ends of the feedline and ~10 wires connecting the ground plane on each side. There are no bond wires across the feedline of the notch, nor any flux trapping holes, which lets the flux to be expelled from the ground plane into the regions of the gap of the coplanar transmission lines. Our experiments were mostly performed on a Bluefors LD400 dilution refrigerator with a base temperature of 10 mK. The employed temperature scale was calibrated against a Coulomb blockade thermometer.[21] The refrigerator has a 4–8 GHz microwave measurement setup, which, in addition to a Low Noise Factory HEMT amplifier, encompasses a Josephson traveling wave parametric amplifier (JTWPA) with nearly quantum limited operation for 4–7 GHz frequency.[22] A diplexer was employed to combine the signal and pumping frequency in the JTWPA. Two 4–8 GHz circulators were installed between the sample and JTWPA, while two 4–12 GHz circulators were employed at the JTWPA output to eliminate any back-propagating pump signal. For further details of the system, we refer to Ref. 23.

The calibration of the input power was performed by measuring the attenuation of the lines at room temperature. This calibration yielded the attenuation of 79.6 dB for the in-going microwave signal around 6 GHz (frequency range of 25 nm thick samples). This attenuation was subtracted from the generator power, which in our experiments was limited to +15 dBm. The calibration was done similarly for the experiments on 10 nm (≃4 GHz) and 105 nm devices (≃7 GHz).

Our notch-type samples have five coplanar and quarter-wave microwave cavities connected capacitively to the measurement line with a separation of ~0.6 mm [see Fig. 1(a)]. The lengths of the $\lambda/4$ cavities vary over 3.86–4.36 mm, which correspond to the design frequency range of $f_{dgn} = 6.83$–7.73 GHz without kinetic inductance. The estimation of kinetic inductance from the experimental results was obtained using the basic equivalent model of the $\lambda/4$ cavity with resonant frequency $2\pi f_m = 1/\sqrt{C(L_{geo} + L_K)}$, where C is the total capacitance, L_{geo} is the total geometric inductance, and L_K is the corresponding kinetic inductance of the coplanar line.

The scattering parameter for transmission, $S_{21}(\omega)$, for a notch type resonator is given by[24–26]

$$S_{21}(\omega) = a e^{i\alpha} e^{-i\omega\tau}\left(1 - \frac{(Q_{load}/|Q_{cpl}|)e^{i\varphi}}{1 + 2iQ_{load}(\omega/\omega_r - 1)}\right), \tag{2}$$

where $a e^{i\alpha} e^{-i\omega\tau}$ quantifies the environment with amplitude a, phase shift α, and electronic delay τ; Q_{load} is the loaded quality factor; $|Q_{cpl}|$ is the absolute value of the coupling quality factor; φ quantifies impedance mismatch; ω is the probing frequency; and ω_r is the resonance frequency. The fitting[27] in Eq. (2) to the measured data yields Q_{cpl} and Q_{load}, which then gives the internal Q_{int} factor using

$$\frac{1}{Q_{int}} = \frac{1}{Q_{load}} - \frac{1}{Q_{cpl}}. \tag{3}$$

In our data on 10 and 105 nm samples, the resistive and reactive responses are somewhat mixed, which requires careful analysis using Eq. (2). In the experiments, the magnitude of the transmission signal is well calibrated so that the parameter $a = 1$ with an error <1%. In addition, the phase of the vector network analyzer (VNA) probing signal is quite well calibrated, and $\omega\tau \ll 1$ in most of our response curve fits, except some fits at large measurement powers (data in the emerging non-linear Duffing regime).

The internal quality factor is expected to be governed by dissipation coming from quasiparticle resistance (qp), two-level tunneling states (TLS), and flux flow (FF),[3]

$$\frac{1}{Q_{int}} = \frac{1}{Q_{qp}} + \frac{1}{Q_{TLS}} + \frac{1}{Q_{FF}}. \tag{4}$$

Here, $Q_{qp} = R_{qp}/\omega L$ with $R_{qp} = R_n \exp(\Delta/k_B T)$ and L is the total inductance, and Q_{TLS} is typically a function of average photon occupation number $\bar{n}$ in the cavity, i.e., $Q_{TLS}(\bar{n})$ with a tendency to lead to an increase in Q with increasing power owing to saturation and a relaxation behavior of the TLSs. The last term in Eq. (4) describes dissipation due to flux influenced by screening currents and defects/pinning centers in the sample.

IV. EXPERIMENTAL RESULTS

The impedance of a notch type of resonator including its environment leads to the scattering parameter S_{21} given by Eq. (2). The measured response curve is shown in Fig. 2(b), in which the large suppression at resonance indicates that our device is nearly critically coupled.

Figure 2 shows fits of Eq. (2) to the measured data in a 25-nm-thick resonator. In both 10- and 105-nm-thick resonators, the real and imaginary components of a Lorentzian response function are strongly mixed, while the mixing is nearly absent in the 25 nm thick cavities. Equation (2) fits our data well in the linear response regime. When approaching the critical drive amplitude for the hysteretic Duffing regime, the fits deteriorate, and they become fully impossible in the hysteretic regime (part of the circle is missing). In addition to the Duffing behavior, the 10 nm samples were found to display heating effects, which led to extra hysteresis due to frequency shifts caused by $L_K(T)$. The analyzed results in this

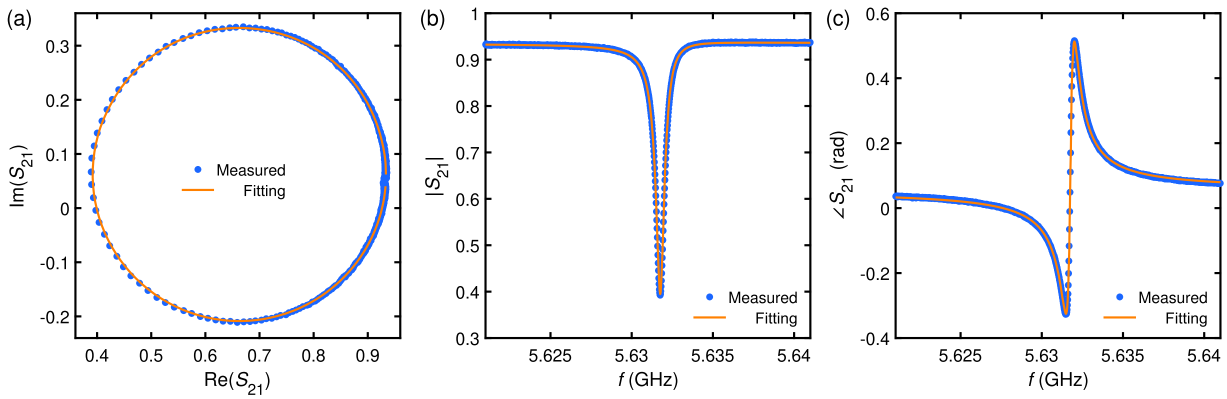

FIG. 2. (a) Notch-type scattering parameter circle for the 25 nm thick $CoSi_2$ cavity measured at 20 mK. (b) and (c) Magnitude and phase response, respectively. The fit curves are calculated using Eq. (2) with parameters $\omega_r/2\pi = 5.632 \times 10^9$ s^{-1}, $Q_{load} = 7092$, $Q_{cpl} = 12\,236$, $\phi = -0.097$ rad, $a = 0.9348$, $\alpha = 0.2939$, and $\tau = 6.767 \times 10^{-12}$ s.

TABLE II. Characteristics of the investigated 25-nm-thick $CoSi_2$ resonators with a nominal characteristic impedance of $Z_0 = \sqrt{L/C} = 50\ \Omega$; actual $Z_0 = 65\ \Omega$. The design frequency f_{dgn} is calculated from the length L_{line} using the theoretical speed of propagation. f_m denotes the measured resonance frequency, which yields the kinetic inductance to the geometric inductance ratio L_K/L_{geo}. Q_{int}, Q_{cpl}, and Q_{load} denote internal, coupling, and loaded quality factors, respectively. These characteristics were measured at $\bar{n} \approx 1000$ average cavity photon occupation number.

	f_{dgn}/GHz	f_m/GHz	L_{line}/mm	L_K/L_{geo}	Q_{int}	Q_{cpl}	Q_{load}
f_1	6.83	5.208	4.36	0.720	6 930	20 910	5200
f_2	7.16	5.447	4.15	0.728	19 170	12 160	7440
f_3	7.38	5.632	4.04	0.717	18 500	12 760	7550
f_4	7.49	5.782	3.91	0.678	28 180	11 880	8360
f_5	7.73	5.882	3.86	0.727	25 560	10 480	7430

work are based on resonance shapes and fits close to those shown in Fig. 2.

Table II presents the fitting results for 25-nm-thick microwave cavities. The design frequencies f_{dgn} reflect the physical length of the resonators and the speed of propagation in the coplanar transmission lines given by $1/\sqrt{\ell c}$, where ℓ and c are the inductance and capacitance per unit length, respectively. Frequency f_m denotes the measured resonance frequency, which yields the ratio of kinetic and geometric inductances as $L_K/L_{geo} = (f_{dgn}/f_m)^2 - 1$. The division of the loaded Q factor into the coupling dissipation rate $\propto 1/Q_{cpl}$ and inherent dissipation rate $\propto 1/Q_{int}$ arises from circle size S_{21} and its orientation given in Eq. (2). The obtained kinetic inductance is consistently around $L_K/L_{geo} = 0.72$, which indicates a pretty uniform quality for the $CoSi_2$ film. For the inherent average dissipation from all data points, we find $Q_{ave} = 19\,700$. However, if we were to neglect the first resonator with a somewhat unrealistic coupling factor, we would find $Q_{ave} = 22\,900$, not far from the full average.

Figure 3(a) shows the kinetic inductance L_K deduced from the resonance frequency of 25 nm thick $CoSi_2$ cavity as a function of temperature. Data obtained at three different measurement powers P_m are given (see the legend for P_m values). Already when $T > 0.1$ K, a distinct change in the temperature-dependent kinetic inductance $L_K(T)$ is observed. The fit illustrates $1/\Delta(T)$ dependence given in Eq. (1) using $L_{geo} \simeq 1.4$ nH and $T_c = 1.15$ K. The substantial deviation from the actual $T_c = 1.31$ K may be an indication that the simple formula $L_K(T) \propto R_n/\Delta(T)$ is not fully accurate in our system. The inset displays the frequency change δf relative to the $T = 0$ value $\delta f/f_0 = |f_m(T) - f_m(0)|/f_m(0)$ vs T on a log–log scale. Our data display power law dependence $\propto T^\alpha$ with an exponent $\alpha = 4.3 \pm 0.2$. This finding differs from the standard behavior of metallic materials with similar sheet resistance,[28] and it calls either for non-BCS mechanisms, for example, triplet type pairing,[15] or a suitable phonon density of states[29] for the creation of elementary excitations.

Figure 3(b) shows the internal quality factor Q_{int} extracted from the same data used for Fig. 3(a) (the legend indicates the values of P_m). The data display a universal exponential behavior at high T: the fitted dashed line depicts the exponential dependence due to quasiparticle dissipation, $Q_{int} \propto R_{qp} \propto \exp(\Delta/k_B T)$ with constant $\Delta/k_B = 1.75$ K. Using the BCS relation $\Delta/k_B = 1.76 T_c$, we obtain $T_c = 0.99$ K. This suppression of apparent T_c indicates either local reduction in the gap at some weakly ordered $CoSi_2$ spots or significant dissipation facilitated by the non-uniform gap in a triplet part of the $CoSi_2$ order parameter.[15]

Owing to large normal state resistance, the cavity frequency in the normal state cannot be measured. Instead, the design frequency (length of cavity) was applied to deduce the frequency shift due to kinetic inductance. Kinetic inductance is found to follow scaling with $1/d$, as in the data shown in Fig. 3(c), which depicts L_K values of all five resonators measured for each thickness. The sample with the largest thickness $d = 105$ nm displays the biggest scatter owing to the uncertainty in determining the normal state frequency and the role that this uncertainty plays in determining the kinetic inductance fraction.

Figure 3(d) shows the internal quality factor as a function of thickness, showing a $d(A - \log d)$ type of dependence. The depen-

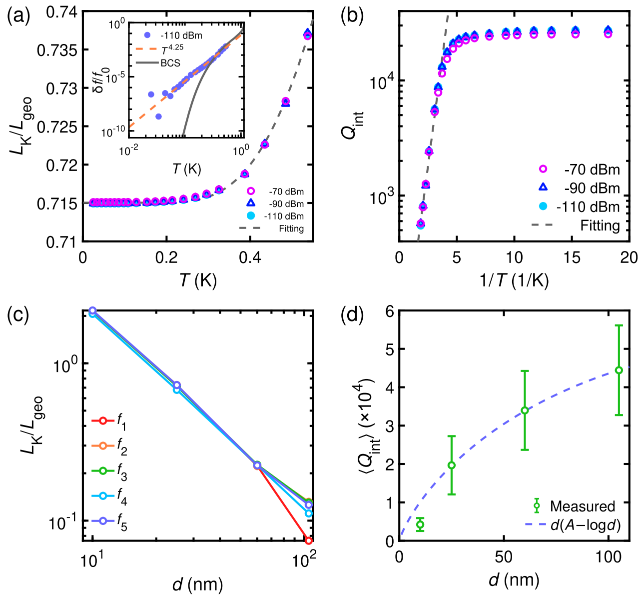

FIG. 3. (a) Kinetic inductance of the 25-nm-thick $CoSi_2$ cavity as a function of temperature. The fit illustrates the $1/\Delta(T)$ dependence given in Eq. (1) with T_c = 1.15 K. The inset shows the scaled resonance frequency shift $\delta f/f_0 = |f_m(T) - f_m(0)|/f_m(0)$ as a function of temperature on the log–log scale. The fitted dashed line yields $\delta f \propto T^{4.25}$. For comparison, the gray curve illustrates the expected behavior by numerically evaluating the BCS energy gap equation with T_c = 1.15 K. (b) Simultaneously measured internal quality factor Q_{int} vs temperature. The line depicts exponential dependence due to quasiparticle dissipation, $\exp(-\Delta/k_B T)$ with constant Δ/k_B = 1.75 K. (c) Kinetic inductance (T = 20 mK) as a function of film thickness d including all the measured cavities. The average data follow the $1/d$ dependence originating from the approximate $R_n \propto 1/d$ relation. (d) Average internal quality factor $\langle Q_{int}\rangle$ vs film thickness d. The dashed line illustrates the fit to $Q \propto \frac{d}{d_0}\left\{\log\left(\frac{j_0}{j_c}\right) - \log\left(\frac{d}{d_0}\right)\right\}$ with $\frac{j_0}{j_c} d_0$ = 572 nm; see the text for details.

dence of the cavity resonance frequency f_m and the inherent quality factor Q_{int} on the drive power P_m (or equivalently, the number of photons in the cavity) is shown in Fig. 4(a). The data display a clear decrease in frequency and increase in dissipation with increasing drive power. We assign most of the increased dissipation to enhanced temperature with smaller quasiparticle resistance R_{qp}. Thus, the measured $f_m(P_m)$ and $Q_{int}(P_m)$ can be employed for thermometric purposes via $f_m(T)$ and $Q_{int}(T)$ dependencies, respectively. The resolution of this kind of thermometry is clearly better using the shift in f_m.

Figure 4(b) shows the electronic temperature T_e obtained from the frequency shift shown in Fig. 4(a) and $f_m(T)$ in the inset of Fig. 3(a), as well as depicts T_e as a function of microwave carrier power P_m. By assuming that all the power will be dissipated in the cavity,[30] the dependence shown in Fig. 4(b) can be employed for the estimation of electron–phonon (e–ph) coupling in this system. Similar estimation of e–ph coupling has been performed, for example, in suspended graphene.[31] A direct power law fit yields for electron–phonon heat flow $\dot{Q} \propto T_e^4$, but one should keep in mind that only a fraction of normal electrons carries the heat (see below).

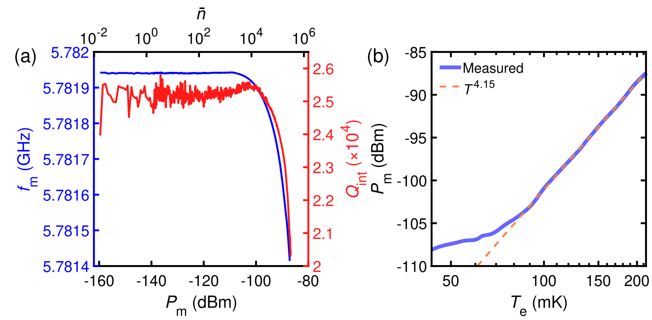

FIG. 4. (a) Power dependence of the cavity frequency f_m (upper curve, left scale) and the internal quality factor Q_{int} (lower curve, right scale). The upper scale indicates the average photon occupation number $\bar{n}$ in the cavity. (b) Electronic temperature T_e (deduced from the data for f_m in frame a) as a function carrier power. The dashed curve is a fit for electron–phonon heat transfer using Eq. (5) with parameters γ = 4.15 and $\rho_n/\rho = 1.0 \times 10^{-3}$.

This power law exponent is close to that found in thermal experiments on a niobium superconductor.[32] We note that the measured dependence $f_m(P_m)$ has a broad, weak maximum around power P_m = −110 dBm. Consequently, the temperature determination from kinetic inductance does not work properly in the range of powers −110 . . . − 105 dBm, resulting in the deviation upward from the fit shown in Fig. 4(b).

Our data on Q_{int} vs P_m also cover small powers [see Fig. 4(a)]. The results showed only a 1%–2% increase in Q_{int} with the number of photons in the range of 1–1000 quanta in the cavity. Consequently, we believe that microwave dissipation due to TLSs is quite small in these $CoSi_2$ devices,[3] which is consistent with the observed extremely limited disorder at the $CoSi_2$/Si interfaces.[9] Most probably, the weak power dependence of $Q_{int}(P_m)$ is due to a small number of TLSs combined with the presence of an extra dissipation channel, e.g., due to flux flow,[33,34] or even more likely, due to driving the boundary layer to a dissipative state by screening currents. We have also performed measurements on frequency fluctuations on these microwave cavities, which corroborate the good quality of this material with a low spectral density of $1/f$ noise in the cavity frequency.[23]

V. DISCUSSION

The given fit curve shown in Fig. 3(d) is based on estimation of the resistance of a dissipative boundary layer induced by screening currents. The screening current density in a superconductor increases exponentially toward the boundary according to $j(x) = j_0 \frac{d_0}{d} \exp(-x/\lambda)$, where x is the distance from the border line, λ is the London penetration depth, and j_0 denotes the current density necessary for flux expulsion at thickness d_0; for non-dissipative expulsion at d_0, j_0 has to be below the critical current density j_c. In the region where critical current density $j_c \sim j(x)$, the state of $CoSi_2$ becomes dissipative. The width of this region is given by $x_n = \lambda \ln\left(\frac{j_0}{j_c}\frac{d_0}{d}\right)$, which yields for the dissipative resistance along the cavity $R = \frac{1}{2}\rho_n \frac{L_{cav}}{x_n d}$. Since a voltage oscillation suffers dissipation $P \propto 1/R$, we obtain for the thickness dependence of the Q factor,

$Q \propto \frac{d}{d_0}\left\{\log\left(\frac{j_0}{j_c}\right) - \log\left(\frac{d}{d_0}\right)\right\}$. This dissipation becomes significant when thickness d is small and the critical current density of $CoSi_2$ is smaller than in Nb at least by a factor of 20.

Our experiments were performed in Earth's magnetic field (~50 μT), which is known to influence cavities made of Al (150 nm thick) and Re (50 nm thick)[34] that are close in characteristics in comparison to our 105 nm devices. The field-induced screening currents at the edges of the superconducting transmission lines will decrease in current density with increasing film thickness. Thus, the ensuing dissipative surface resistance becomes enhanced, leading to smaller dissipation at larger d, as seen in the experiments. The fit shown in Fig. 3(d) yields $d_0 \simeq 600$ nm, which provides an estimate for the thickness of the $CoSi_2$ layer, which would be insensitive to Earth's magnetic field in our geometry.[35] However, further experiments are needed to separate the effect of TLS-based dissipation from flux-based dissipation in our devices.

For normal electrons in metals, the heat transfer by electron–phonon coupling can be written as[36–39]

$$\dot{Q} \simeq \Sigma V_n (T_e^\gamma - T_{ph}^\gamma), \tag{5}$$

where the parameter $\Sigma \simeq 10^9$ W m^{-3} K^{-5} for bulk metals with $\gamma = 5$[40] and $V_n = (\rho_n/\rho)V$ is the effective volume of heat-carrying electrons (fractional density ρ_n/ρ) in total volume V, while T_e and T_{ph} are the electron and phonon temperatures, respectively. In disordered, thin conductors, the exponent γ depends on the disorder and phonon dimensionality, resulting in $\gamma = 4$–6.[41–43]

We obtained exponent $\gamma = 4.15$ by fitting Eq. (5) to the measured $\dot{Q}(T_e)$ shown in Fig. 4(b) using $\rho_n/\rho = 1.0 \times 10^{-3}$, $V = 1.25 \times 10^{-15}$ m^3 for the cavity volume, and $\Sigma \simeq 10^9$ W m^{-3} K$^{-4.15}$. The employed prefactor Σ corresponds to the regular results on metals around 1 K temperature (see, e.g., Ref. 40). The residual normal electron fraction corresponds to $T = 0.25$ K ($T = 0.33$ K) if considered as thermally excited quasiparticles in the sample using $\Delta/k_B = 1.75$ K ($\Delta/k_B = 2.3$ K using $T_c = 1.31$ K), which is clearly higher than the lower range of temperatures in 100–200 mK. This discrepancy in comparison with the typical excess quasiparticle density[44,45] may indicate the presence of anisotropic triplet correlations in $CoSi_2$[15] or an additional relaxation channel from $CoSi_2$ electrons to substrate phonons.[46]

We also estimated the e–ph coupling from 10 to 105 nm samples. However, the results were much more unreliable compared to the 25 nm data. The data on 10 nm cavities were hampered by the small Q factor and an early onset of non-linear behavior, while the resolution of kinetic inductance thermometry in 105 nm devices was bad from the beginning. Thus, we are not able to conclude anything about the universality of the exponent $\gamma = 4.15$ as a function of thickness, which would illuminate the issue of mixed-dimensionality phonons in thin films.[47]

To conclude, our study shows that $CoSi_2$ is a promising material for quantum circuits due to its high-quality, low-temperature superconducting properties, and excellent lattice match to silicon. We demonstrate that thin $CoSi_2$ films possess a substantial kinetic inductance, which displays a non-BCS power-law dependence $\delta L_K \propto T^{4.3\pm0.2}$ at the lowest temperatures. Our investigation also addresses the potential issue of enhanced dissipation at microwave frequencies caused by two-level tunneling states, as well as the efficiency of thermalization of charge carriers at large drives. Our findings suggest that $CoSi_2$ is a valuable addition to the toolkit of materials for quantum circuit fabrication, with applications in ultra-low temperature sensing, single photon detection, and parametric amplification, all providing uses in which strong coupling to the environment can be used to facilitate operation even without shielding from Earth's magnetic field.

ACKNOWLEDGMENTS

We thank Tero Heikkilä, Alexander Zyuzin, Teun Klapwijk, Manohar Kumar, Päivi Törmä, and Shao-Pin Chiu for fruitful discussions and Pei-Ling Wu and Shouray Kumar Sahu for experimental assistance. This work was supported by the Academy of Finland (AF) Project Nos. 341913 (EFT), 312295 and 352926 (CoE, Quantum Technology Finland), and Taiwan–Finland AF mobility Grant No. 341884 (S. S. Yeh). The research leading to these results received funding from the European Union's Horizon 2020 Research and Innovation Programme, under Grant No. 824109 (EMP). Our work was also supported by funding from the Jane and Aatos Erkko Foundation and the Keele Foundation (SuperC project). This experimental work benefited from the Aalto University OtaNano/LTL infrastructure. J. J. Lin acknowledges the support from the National Science and Technology Council (NSTC) of Taiwan through Grant Nos. 110-2112-M-A49-015 and 111-2119-M-007-005. S. S. Yeh acknowledges the support from the NSTC of Taiwan through Grant No. 110-2112-M-A49-033-MY3 and the support from the Taiwan Ministry of Education through the Higher Education Sprout Project of the NYCU.

AUTHOR DECLARATIONS

Conflict of Interest

The authors have no conflicts to disclose.

Author Contributions

Ekaterina Mukhanova: Data curation (equal); Investigation (equal); Methodology (lead); Writing – review & editing (equal). **Wei-jun Zeng**: Data curation (lead); Investigation (equal); Methodology (equal); Writing – review & editing (equal). **Elica Anne Heredia**: Data curation (supporting); Methodology (equal). **Chun-Wei Wu**: Data curation (supporting); Methodology (equal). **Ilari Lilja**: Data curation (equal); Investigation (equal); Methodology (lead); Supervision (supporting); Writing – review & editing (equal). **Juhn-Jong Lin**: Conceptualization (equal); Investigation (equal); Supervision (equal); Writing – review & editing (supporting). **Sheng-Shiuan Yeh**: Conceptualization (lead); Investigation (equal); Methodology (equal); Supervision (equal); Writing – review & editing (equal). **Pertti Hakonen**: Conceptualization (lead); Funding acquisition (equal); Supervision (equal); Writing – original draft (equal); Writing – review & editing (lead).

DATA AVAILABILITY

The data that support the findings of this study are available from the corresponding author upon reasonable request.

REFERENCES

[1] A. Blais, A. L. Grimsmo, S. M. Girvin, and A. Wallraff, Rev. Mod. Phys. **93**, 025005 (2021).

[2] G. Falci, P. J. Hakonen, and E. Paladino, in *Encyclopedia of Condensed Matter Physics*, 2nd ed., edited by T. Chakraborty (Academic Press, Oxford, 2024), pp. 1003–1017.

[3] C. R. H. McRae, H. Wang, J. Gao, M. R. Vissers, T. Brecht, A. Dunsworth, D. P. Pappas, and J. Mutus, Rev. Sci. Instrum. **91**, 091101 (2020).

[4] N. P. de Leon, K. M. Itoh, D. Kim, K. K. Mehta, T. E. Northup, H. Paik, B. S. Palmer, N. Samarth, S. Sangtawesin, and D. W. Steuerman, Science **372**, eabb2823 (2021).

[5] S. Tolpygo, V. Bolkhovsky, T. Weir, A. Wynn, D. Oates, L. Johnson, and M. Gouker, IEEE Trans. Appl. Supercond. **26**, 1100110 (2016).

[6] L. J. Chen, *Silicide Technology for Integrated Circuits* (IET, 2004), Vol. 5.

[7] T. D. Vethaak, "Silicide-based Josephson field effect transistors for superconducting qubits," Ph.D. thesis, Univervity of Grenoble, 2022.

[8] M. Schwarz, T. D. Vethaak, V. Derycke, A. Francheteau, B. Iniguez, S. Kataria, A. Kloes, F. Lefloch, M. Lemme, J. P. Snyder, W. M. Weber, and L. E. Calvet, Nanotechnology **34**, 352002 (2023).

[9] S.-P. Chiu, S.-S. Yeh, C.-J. Chiou, Y.-C. Chou, J.-J. Lin, and C.-C. Tsuei, ACS Nano **11**, 516 (2017).

[10] C. Müller, J. H. Cole, and J. Lisenfeld, Rep. Prog. Phys. **82**, 124501 (2019).

[11] B. Ho Eom, P. K. Day, H. G. LeDuc, and J. Zmuidzinas, Nat. Phys. **8**, 623 (2012).

[12] S. Chaudhuri, D. Li, K. D. Irwin, C. Bockstiegel, J. Hubmayr, J. N. Ullom, M. R. Vissers, and J. Gao, Appl. Phys. Lett. **110**, 152601 (2017).

[13] A. Bezryadin, *Superconductivity in Nanowires: Fabrication and Quantum Transport* (Wiley VCH, 2013), p. 252.

[14] M. Tinkham and C. N. Lau, Appl. Phys. Lett. **80**, 2946 (2002).

[15] S.-P. Chiu, C. C. Tsuei, S.-S. Yeh, F.-C. Zhang, S. Kirchner, and J.-J. Lin, Sci. Adv. **7**, eabg6569 (2021).

[16] K. Maki, Prog. Theor. Phys. **29**, 10 (1963).

[17] A. J. Annunziata, D. F. Santavicca, L. Frunzio, G. Catelani, M. J. Rooks, A. Frydman, and D. E. Prober, Nanotechnology **21**, 445202 (2010).

[18] T. Kikkawa, K. Inoue, and K. Imai, *Cobalt Silicide Technology* (Institution of Engineering and Technology, 2004), pp. 77–94.

[19] L. P. Ren and K. N. Tu, *Silicide Technology for SOI Devices* (Institution of Engineering and Technology, 2004), pp. 201–228.

[20] S.-P. Chiu, C.-J. Wang, Y.-C. Lin, S.-T. Tu, S. Sahu, R.-T. Wang, C.-Y. Wu, S.-S. Yeh, S. Kirchner, and J.-J. Lin, "Electronic conduction and superconducting properties of $CoSi_2$ films on silicon—An unconventional superconductor with technological potential," arXiv:2401.17601 [cond-mat.supr-con] (2024).

[21] J. P. Pekola, K. P. Hirvi, J. P. Kauppinen, and M. A. Paalanen, Phys. Rev. Lett. **73**, 2903 (1994).

[22] M. Perelshtein, K. Petrovnin, V. Vesterinen, S. Hamedani Raja, I. Lilja, M. Will, A. Savin, S. Simbierowicz, R. Jabdaraghi, J. Lehtinen, L. Grönberg, J. Hassel, M. Prunnila, J. Govenius, G. Paraoanu, and P. Hakonen, Phys. Rev. Appl. **18**, 024063 (2022).

[23] W. Zeng, I. Lilja, E. Mukhanova, E. A. Heredia, C.-W. Wu, J.-J. Lin, S.-S. Yeh, and P. Hakonen, "1/f frequency fluctuations due to kinetic inductance in CoSi2 microwave cavities," arXiv:2403.08347 (2024).

[24] J. Gao, "The physics of superconducting microwave resonators," Ph.D. thesis, California Institute of Technology, 2008.

[25] M. S. Khalil, M. J. A. Stoutimore, F. C. Wellstood, and K. D. Osborn, J. Appl. Phys. **111**, 054510 (2012).

[26] S. Probst, F. B. Song, P. A. Bushev, A. V. Ustinov, and M. Weides, Rev. Sci. Instrum. **86**, 024706 (2015).

[27] sebastianprobst/resonator_tools, *A small GitHub library in python to fit complex notch-type resonator scattering data in transmission, reflection measurements*, 2023.

[28] P. C. J. J. Coumou, E. F. C. Driessen, J. Bueno, C. Chapelier, and T. M. Klapwijk, Phys. Rev. B **88**, 180505 (2013).

[29] G. M. Eliashberg, G. V. Klimovitch, and A. V. Rylyakov, J. Supercond. **4**, 393 (1991).

[30] There is no galvanic contact facilitating electronic heat conduction away from the cavity.

[31] A. Laitinen, M. Oksanen, A. Fay, D. Cox, M. Tomi, P. Virtanen, and P. J. Hakonen, Nano Lett. **14**, 3009 (2014).

[32] A. V. Feshchenko, O. P. Saira, J. T. Peltonen, and J. P. Pekola, Sci. Rep. **7**, 41728 (2017).

[33] M. W. Coffey and J. R. Clem, Phys. Rev. B **46**, 11757 (1992).

[34] C. Song, T. W. Heitmann, M. P. Defeo, K. Yu, R. McDermott, M. Neeley, J. M. Martinis, and B. L. Plourde, Phys. Rev. B **79**, 174512 (2009).

[35] The mean free path influences the kinetic inductance via the normal state resistance. Also, the coherence length in the dirty limit depends on the mean free path. These quantities describe the superconductor response and they do not lead to a change in dissipation. The surface resistance of a superconductor $R_s \propto l_{mfp} \exp(-\Delta/k_B T)$ which means that the resistance of the cavity inductance goes down with the mean free path. An equivalent model of this is an parallel *RLC* circuit where $R = R_s(1 + Q^2)$ where $Q = \omega L/R_s$. Hence, the smaller the mean free path, the less the R_s, and the larger the R. Consequently, the smaller the l_{mfp}, the smaller the dissipation, which is contrary to the observations.

[36] A. V. Sergeev and M. Yu Reizer, Int. J. Mod. Phys. B **10**, 635 (1996).

[37] A. V. Timofeev, C. P. García, N. B. Kopnin, A. M. Savin, M. Meschke, F. Giazotto, and J. P. Pekola, Phys. Rev. Lett. **102**, 017003 (2009).

[38] T. T. Heikkilä, R. Ojajärvi, I. J. Maasilta, E. Strambini, F. Giazotto, and F. S. Bergeret, Phys. Rev. Appl. **10**, 034053 (2018).

[39] D. Nikolic, D. M. Basko, and W. Belzig, Phys. Rev. B **102**, 214514 (2020).

[40] F. Giazotto, T. T. Heikkilä, A. Luukanen, A. M. Savin, and J. P. Pekola, Rev. Mod. Phys. **78**, 217 (2006).

[41] M. L. Roukes, M. R. Freeman, R. S. Germain, R. C. Richardson, and M. B. Ketchen, Phys. Rev. Lett. **55**, 422 (1985).

[42] A. Sergeev and V. Mitin, Phys. Rev. B **61**, 6041 (2000).

[43] J. T. Karvonen, L. J. Taskinen, and I. J. Maasilta, Phys. Rev. B **72**, 012302 (2005).

[44] P. J. de Visser, J. J. A. Baselmans, S. J. C. Yates, P. Diener, A. Endo, and T. M. Klapwijk, Appl. Phys. Lett. **100**, 162601 (2012).

[45] P. J. de Visser, D. J. Goldie, P. Diener, S. Withington, J. J. A. Baselmans, and T. M. Klapwijk, Phys. Rev. Lett. **112**, 047004 (2014).

[46] T. Elo, P. Lähteenmäki, D. Golubev, A. Savin, K. Arutyunov, and P. Hakonen, J. Low Temp. Phys. **189**, 204 (2017).

[47] D. V. Anghel, C. Caraiani, and Y. M. Galperin, Phys. Scr. **94**, 105704 (2019).

[48] We can approximately estimate the capacitance of the coplanar conductor as that of two parallel wires (bottom ground plane is far away), for which it is known that $C \propto 1/\log(2a/d)$ where a is the separation of wires with diameter d. Modeling dissipation as R in parallel to C, the effective Q factor of the capacitance is given by $Q = \omega CR$, which yields $Q \propto \log(d)$ in the first order expansion when $d \ll a$. However, the change in Q in this model would not be as large as observed in the experiment.